Steady-state Flow Solutions for Delta Wing Configurations at High Angle of Attack using Implicit Schemes

Arpit Aggarwal, Ralf Hartmann, Stefan Langer, Tobias Leicht

German Aerospace Center, Member of the Helmholtz Association, Institute of Aerodynamics and Flow Technology, Lilienthalplatz 7, 38108 Braunschweig, Germany.
arpit.aggarwal@dlr.de, ralf.hartmannn@dlr.de, stefan.langer@dlr.de, tobias.leicht@dlr.de

Abstract. Finding fully converged, steady-state solutions of the compressible Reynolds Averaged Navier-Stokes (RANS) equations for aerodynamic configurations on the border of the flight envelope often poses serious challenges to solution algorithms that have proven robust and successful for configurations at cruise conditions. Examples of such cases are agile configurations at high angles of attack. When trying to compute solutions in these scenarios, one often observes that the solution process breaks down after few iterations or that a steady-state RANS solution, although it may exist, cannot be reached with the employed solution algorithm. While, in general, no clear reason for this behavior can be identified, the complexity of these flows seems to be significantly greater compared to flows around transport aircraft in cruise flight. The flow fields are dominated by the interaction of shock waves with a system of vortices emanating from the leading edges on the upper surface of the wing, leading to massive flow separation. These flow features tend to be inherently unsteady and can be assumed to cause problems in computing a converged solution using an algorithm designed to find steady-state solutions of the RANS equations. To avoid these problems, it is not uncommon to calculate such configurations in an unsteady mode, which often comes at a rather high computational cost. This article demonstrates the necessity for implicit smoothers to approximate fully converged solutions of these challenging simulations. A numerical example is given to confirm that convergence is only possible using an exact derivative together with a suited preconditioner.

1 Introduction, governing equations and discretization

1.1 Introduction

To approximate steady-state solutions of the turbulent compressible Reynolds averaged Navier-Stokes (RANS) equations multistage Runge-Kutta methods are established as smoothing techniques within a Full-Approximation Storage (FAS) multigrid method [1]. In the literature of Computational Fluid Dynamics (CFD) many acceleration and stabilization techniques have been suggested to improve the basic multistage scheme, for example explicit local time stepping [2], point and line implicit methods [3–6] as well as methods exploiting specific approximations to the full derivative or even using the

This is an Author Accepted Manuscript version of the following chapter: Arpit Aggarwal, Ralf Hartmann, Stefan Langer and Tobias Leicht, Steady-State Flow Solutions for Delta Wing Configurations at High Angle of Attack Using Implicit Schemes, published in New Results in Numerical and Experimental Fluid Mechanics XIII, edited by Andreas Dillmann, Gerd Heller, Erwald Krmer and Claus Wagner, 2021, Springer reproduced with permission of Springer Nature Switzerland AG. The final authenticated version is available online at: https://doi.org/10.1007/978-3-030-79561-0_26

full derivative combined with an iterative solution method approximating the solution to the linear systems [7]. In general, smoothers having a large amount of implicitness have proven to be more successful compared to explicit or weakly implicit ones. A complete overview of how the various Runge-Kutta smoothers are related can be found in [8].

Although implicit smoothers have proven their potential for many examples, for configurations on the border of the flight envelope one often observes severe difficulties to reliably approximate a steady-state solution. This suggests that further parameters influencing the overall iterative process need to be investigated for increased robustness. For example, each iterative solution process for nonlinear equations starts from an initial guess, typically the free-stream. For complex flow fields, however, the free-stream can be far away from the final solution. Thus, it is not unexpected that simple globalization strategies – even if they work well for smooth flows – are no longer able to find a valid solution path from the initial guess to the final result when applied to flows at the border of the flight envelope.

This article discusses and extends implicit smoothers by globalization (also called regularization) methods to prevent divergence in the beginning of the nonlinear iteration process, in order to overcome the problem of not having a good initial guess. Proposed methods exploit CFL number ramping strategies together with the choice of the underlying time step. Furthermore, a comparative study is performed between these methods and unsteady computations on the same configuration.

1.2 RANS equations and Discretization

For an open domain $\Omega \subset \mathbb{R}^3$ the three-dimensional RANS equations are considered in conservative variables $\mathbf{W} := (\rho, \rho u_1, \rho u_2, \rho u_3, \rho E)$ written as

$$\frac{\mathrm{d}}{\mathrm{d}t} \int_{\Omega} \mathbf{W} \, \mathrm{d}\mathbf{x} + \int_{\partial\Omega} \left(\mathbf{f}_c \cdot \mathbf{n} - \mathbf{f}_v \cdot \mathbf{n} \right) \, \mathrm{d}s = 0. \tag{1}$$

Turbulence is modeled using the one-equation turbulence model introduced by Spalart and Allmaras [9, 10]. The additional equation is given by

$$\frac{\mathrm{d}}{\mathrm{d}t} \int_{\Omega} \tilde{\nu} \, \mathrm{d}\mathbf{x} + \int_{\partial\Omega} \left(\mathbf{f}_{c,turb} \cdot \mathbf{n} - \mathbf{f}_{v,turb} \cdot \mathbf{n} \right) \, \mathrm{d}s(y) = \int_{\Omega} Q \, \mathrm{d}\mathbf{x}. \tag{2}$$

The eddy viscosity μ_t is computed by $\mu_t := \rho \tilde{\nu} f_{\mathrm{v}_1}$ where $f_{\mathrm{v}_1} := \frac{\chi^3}{\chi^3 + c_{\mathrm{v}_1}^3}$, $\chi := \frac{\tilde{\nu}}{\nu_l}$, $\nu_l := \frac{\mu_l}{\rho}$. The definition of the convective terms $\mathbf{f}_c \cdot \mathbf{n}$ and $\mathbf{f}_{c,turb} \cdot \mathbf{n}$, viscous terms $\mathbf{f}_v \cdot \mathbf{n}$ and $\mathbf{f}_{v,turb} \cdot \mathbf{n}$ and the source terms Q can be found for example in [9, 10]. For the results given in this article the recommendations concerning the turbulence model given in [10] are followed.

A finite volume formulation on median dual grids is employed as spatial discretization. Control volumes are defined around the vertices of the primary grids. The inviscid terms are discretized using a central difference scheme with an added matrix valued artificial dissipation [11]. A first order Roe scheme or a second order central difference scheme is applied for the convective part of the turbulence model (2). Gradients required for the viscous terms and for the source terms are computed using a Green-Gauss formulation (see [12]). For a detailed description of the discretization strategy and boundary conditions applied refer to [11, 13].

2 Solution method

2.1 Implicit smoother

After discretization one obtains the system of ordinary differential equations

$$\frac{d\mathbf{W}}{dt} = -\mathbf{M}^{-1}\mathbf{R}(\mathbf{W}) \qquad \text{where} \quad \mathbf{M} := \text{diag}\left(\text{diag}\left(\text{vol}(\Omega_i)\right)\right). \tag{3}$$

To approximate a steady-state solution of (3), a multistage diagonally implicit Runge-Kutta method is applied to obtain the smoother (see [8])

$$\begin{aligned} \mathbf{W}^{(0)} &:= \mathbf{W}^n \\ \mathbf{W}^{(j)} &= \mathbf{W}^{(0)} - \alpha_{j+1,j}\mathbf{P}_j\left(\mathbf{W}^{(j-1)}\right)^{-1}\mathbf{R}\left(\mathbf{W}^{(j-1)}\right), \quad j = 1,\ldots,s \qquad (4) \\ \mathbf{W}^{n+1} &= \mathbf{W}^{(s)}, \end{aligned}$$

$$\mathbf{P}_j\left(\mathbf{W}^{(j-1)}\right) := (\Delta T)^{-1}\mathbf{M} + \frac{d\mathbf{R}}{d\mathbf{W}}\left[\mathbf{W}^{(j-1)}\right], \quad \Delta T := \text{diag}\left(\text{diag}\left(\Delta t_i\right)\right). \tag{5}$$

To realize (4), the linear equation $\mathbf{P}_j x = \alpha_{j+1,j}\mathbf{R}\left(\mathbf{W}^{(j-1)}\right)$ needs to be solved. A left or right preconditioned Generalized Minimal Residual (GMRes) method [14] is used,

$$\mathbf{Prec}_j^{-1}\mathbf{P}_j\mathbf{x} = \alpha_{j+1,j}\mathbf{Prec}_j^{-1}\mathbf{R}(\mathbf{W}^{(j-1)}), \tag{6}$$

$$\mathbf{P}_j\mathbf{Prec}_j^{-1}\mathbf{u} = \alpha_{j+1,j}\mathbf{R}(\mathbf{W}^{(j-1)}), \quad \mathbf{u} = \mathbf{Prec}_j\mathbf{x}. \tag{7}$$

Here $\mathbf{Prec}_j$ denotes a preconditioner. Then, for each step in the GMRes method, a symmetric Gauss-Seidel method is applied to approximate a solution of

$$\mathbf{Prec}_j\mathbf{w} = \mathbf{P}_j\mathbf{v}_k \tag{8}$$

where $\mathbf{V}_m = (\mathbf{v}_1,\ldots,\mathbf{v}_m)$ is the Krylov subspace. The key ingredient is the design of the preconditioner. In the following, two different strategies are proposed.

2.2 Preconditioning strategies

Strategy 1: The matrix-free approach implements the preconditioner by a lower-upper symmetric Gauss-Seidel (LU-SGS) scheme, that is

$$\mathbf{Prec}_j = (\Delta T)^{-1}\mathbf{M} + \frac{d\mathbf{R}^{1st,scalar}}{d\mathbf{W}}$$

and $\frac{d\mathbf{R}^{1st,scalar}}{d\mathbf{W}}$ is a scalar, compact approximation to $\frac{d\mathbf{R}}{d\mathbf{W}}$ (see [13] for details). To approximately solve the linear systems (8) by a symmetric Gauss-Seidel method the number of forward and backward sweeps can be varied.

Strategy 2: In the second approach the preconditioner is given by

$$\mathbf{Prec}_j = (\Delta T)^{-1}\mathbf{M} + \frac{d\mathbf{R}^{1st}}{d\mathbf{W}}, \tag{9}$$

where $\frac{d\mathbf{R}^{1st}}{d\mathbf{W}}$ is a linearization of a residual based on a first-order discretization using a compact stencil. Then, the linear systems (8) are approximately solved by application of a line-symmetric Gauss-Seidel method.

Remark: For zero steps of the actual GMRes iteration, **Strategy 1** reduces to the LU-SGS method suggested by Yoon and Jameson [15], while **Strategy 2** yields the methods suggested in [7, 11].

2.3 Approximation of Jacobian

Within the GMRes method the matrix-vector multiplication of the operator given in (5) applied to a vector is approximated by a finite difference of the residual operator,

$$\frac{d\mathbf{R}}{d\mathbf{W}}(\mathbf{W})\,\mathbf{h} \approx \frac{1}{\varepsilon_2 - \varepsilon_1}\left(\mathbf{R}\left(\mathbf{W} + \varepsilon_2 \mathbf{h}\right) - \mathbf{R}\left(\mathbf{W} + \varepsilon_1 \mathbf{h}\right)\right).$$

For $\varepsilon_2 = -\varepsilon_1 = \varepsilon > 0$ one obtains a symmetric finite difference, while $\varepsilon_2 = \varepsilon > 0$ and $\varepsilon_1 = 0$ yields a computationally cheaper forward difference. The choice of a suitable ε is not trivial, as cancellation and approximation errors need to be balanced. A possible method can be found in [12, Chapter 6.2.5].

2.4 Choice of time step, stabilization

As a general rule, time step sizes and thus CFL numbers should be chosen smaller (for robustness) in the beginning and larger (for efficiency) in the final phases of the nonlinear solution process. It turns out that for flows at the border of the flight envelope, such as delta wings at high angle of attack, a simple CFL number ramping strategy such as [11]

$$\mathrm{CFL}\,(n) = \min\left\{\mathrm{CFL}_{\mathrm{init}} \cdot f(n), \mathrm{CFL}_{\max}\right\}, \quad f(n) = \begin{cases} 1, & n < 10, \\ \gamma^{n-10}, & n \geq 10, \end{cases} \qquad \gamma > 1, \quad (10)$$

sometimes fails and the iteration diverges. Instead, in particular for the initial phase of the algorithm where the initial guess $\mathbf{W}_\infty$ (i.e. the free-stream) is far away from the solution, two different strategies are proposed.

Strategy 1: The matrix of local time steps Δt is replaced by

$$\Delta T^{\mathrm{global}} := \mathrm{diag}\left(\mathrm{diag}\left(\Delta t_{\min}\right)\right), \qquad \Delta t_{\min} = \min\left\{\Delta t_i : i = 1, \ldots N\right\}. \qquad (11)$$

Here Δt_i denotes the local time step determined by the spectral radius of local derivatives [8] and N the number of grid points. Then, the Runge-Kutta smoother may be interpreted as a kind of Rosenbrock-method with a global time step $\Delta t_{\min}$. During the iteration the CFL number might be increased carefully. After a certain number of initial steps the matrix of global time steps can be replaced by local time steps, to speed up the convergence rate.

Strategy 2: The global time step choice (11) is a straightforward idea, but can be computationally expensive, in the sense that it can lead to an overly careful approach, which then requires unreasonably many initial steps. Hence, the idea is to use a CFL ramping strategy, which is not as aggressive as (10), in particular in the starting phase, but which is also not as careful as (11), via including a feedback mechanism to detect emerging divergence. Here, the Switched Evolution Relaxation (SER) [16] technique is proposed to increase the CFL number. Then the mapping $f(n)$ in (10) is given by

$$f(n) = \left(q(n)\right)^{\alpha}, \qquad q(n) := \left\|\mathbf{R}\left(\mathbf{W}_\infty\right)\right\|_2 / \left\|\mathbf{R}\left(\mathbf{W}^n\right)\right\|_2, \qquad (12)$$

where α is a free parameter. Assuming convergence ($\left\|\mathbf{R}\left(\mathbf{W}^n\right)\right\|_2 \to 0$, $n \to \infty$) $q(n) \to \infty$, $n \to \infty$ is obtained, and the rate depends on the convergence rate of

$(\|\mathbf{R}(\mathbf{W}^n)\|_2)_{n\in\mathbb{N}}$. Hence, the SER technique (12) relates the increase in CFL to the convergence rate of the global normalized residual $q(n)$. As the residual decreases or increases with the iterations, this feedback is looped into the calculation of the increase of CFL. CFL_{max} in (10) is kept at a very high value of about 10^{10} despite the demanding nature of the considered configurations. The parameter α controls damping and smoothing in the initial phase. For large-scale 3D turbulent flows a choice of $\alpha = 2/5$ is used, as in the examples presented here. For simpler cases, as 2D flows, a larger value of α is often possible.
Additionally, to further improve robustness, solver recovery techniques are implemented to monitor, restore and repeat the solution process with a reduced CFL number, for the case that the SER technique has increased the CFL number too large or too quickly.

3 Numerical results

3.1 Transonic flow over a delta-wing with attached sting

As a first example, a transonic flow around a $65°$ sweep angle delta wing geometry with attached sting from the *Second Vortical Flow Experiment (VFE-2)* [17, 18] is considered with following inflow conditions: Mach number $\mathbf{Ma} = \mathbf{0.869}$, angle of attack $\mathbf{AoA} = \mathbf{24.7}°$ and Reynolds number $\mathbf{Re} = \mathbf{59.5} \times \mathbf{10^6}$. This case is solved on a sequence of three mixed-element meshes including tetrahedra, hexhedra, prisms and pyramids. The number of nodes are about $\mathbf{4.6} \times \mathbf{10^6}$, $\mathbf{10.0} \times \mathbf{10^6}$ and $\mathbf{30.9} \times \mathbf{10^6}$ computed in parallel with 32, 64 and 96 partitions, respectively. A plot of the geometry with mesh topology is given in Figure 2. Figure 1 hints at the complexity of the

Grid	LU-SGS	Strat.1
1	22.6h	23.3h
2	56.7h	176.7h
3	228.7h	1729h

Table 1. Time taken to achieve convergence.

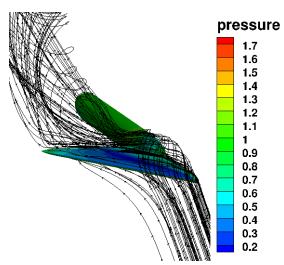

Fig.1. Pressure distribution with streamlines

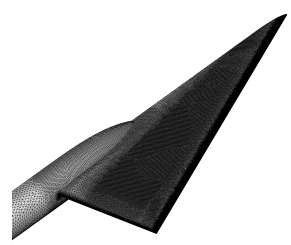

Fig.2. Delta wing with attached sting.

solution of the RANS equations for this configuration. A lambda-shock is seen on the upper surface of the wing. A large vortex and flow separation is observed downstream. The interaction of these flow phenomena yields a complex flow topology around the geometry and may lead to a breakdown of weak solution algorithms.

To find a steady state solution, a Full-Multigrid (FMG) method is employed together with **Strategy 1** from section 2.2 using five levels of grid coarsening. The SER technique (12) is used to increase the CFL number from a starting value of 1. The computations are compared with the LU-SGS method (the legacy solution method in

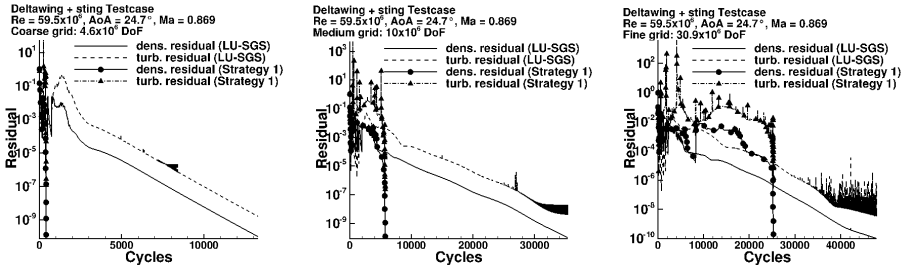

(a) Grid 1, 4.6×10^6 nDoF (b) Grid 2, 10.0×10^6 nDoF (c) Grid 3, 30.9×10^6 nDoF

Fig. 3. Residual convergence for delta-wing with attached sting using **Strategy 1** from section 2.2.

the DLR TAU-Code [13]). The latter smoother represents a compromise between acceptable robustness for a large number of test cases, and a small amount of work per iteration. On the other hand, for complex flows and a significant increase in mesh size this method often fails to find steady state solutions. Comparisons of the convergence histories are shown in Figure 3. The iterations are stopped when the density residual dropped below 10^{-10}, which is reached for both methods. The residual of the turbulence flow equation stagnates for the LU-SGS method on the finer meshes, a hint for a lack of robustness. Although the number of multigrid cycles until convergence is lower for **Strategy 1** from Section 2.2, the effort per iteration is significantly greater, leading to an increase in computational time, shown in Table 1. Strictly speaking, such a comparison is not really valid, since no convergence is achieved for the LU-SGS method (regarding the turbulent flow equation). Furthermore, no particular emphasis has been put into optimizing the solver parameters. In particular, on the finer meshes there might be plenty of room for efficiency improvements of **Strategy 1**, for example, considering nonblocking communication and pipelining [19] as well as shifting some work from outer Krylov iterations to inner preconditioner iterations, cf. Section 3.2.

Figure 4 shows a comparison of the computed pressure coefficient C_p and the experimental data [20] over the wing surface at locations $X/c_R = 0.2, 0.6,$ and 0.95 (see [20]). Figure 4(a) shows a reasonable agreement in the two data-sets, except that the computed results predict the shockwave slightly later than the experimental findings. Moving downstream, in Figures 4(b) and 4(c), the experimental and computational data show a significant offset on the upper surface of the wing. Possible reasons for these deviations are e.g. errors introduced by the turbulence model, missing mesh resolution, and uncertainties in the measurements. An overprediction of vorticity is also a possible known contributing factor. However, the qualitative behavior is roughly similar while both the CFD results are identical and lie on top of each other.

3.2 Low Mach flow over a delta-wing with load

As a second example, a delta-wing with an attached missile and a deployed slat (Figure 5) is considered at a low inflow Mach number $\mathbf{Ma} = \mathbf{0.15}$, a high angle of attack $\mathbf{AoA} = \mathbf{20}^\circ$ and the Reynolds number $\mathbf{Re} = \mathbf{3.4} \times \mathbf{10^6}$. The approximation of

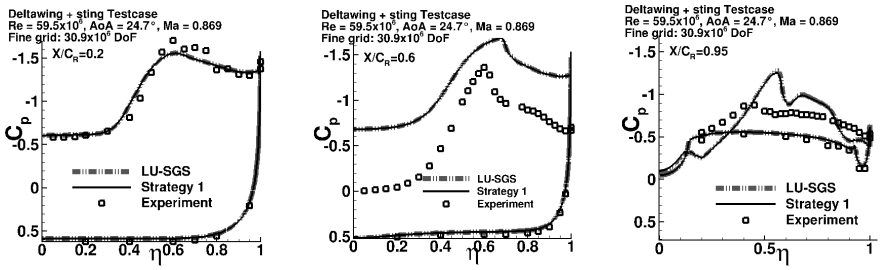

(a) $X/c_R = 0.2$ (b) $X/c_R = 0.6$ (c) $X/c_R = 0.95$

Fig. 4. Comparison of C_p distribution over wing surface between CFD and experimental results.

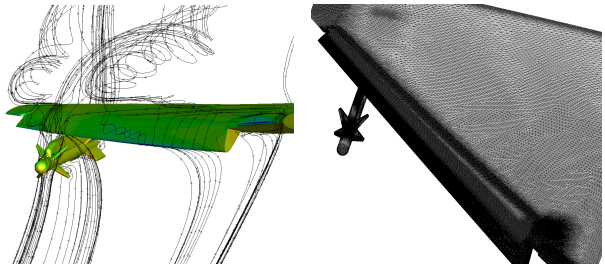

(a) Pressure distribution with streamlines (b) Mesh topology

Fig. 5. Delta wing with load.

steady-state solutions for such low speed cases is often not straightforward due to the high complexity of the associated flow fields, which are often characterized by large regions of separation as well as a mixture of local compressibility effects with incompressible flow dominating major parts of the domain as seen in Figure 5(a) [21]. Thus, solution methods based on simplifications of the smoother (4) can fail.

To confirm this conjecture, for a coarse mesh with about $\mathbf{5.5 \times 10^6}$ degrees of freedom (nDoF), **Strategy 2** from Section 2.2 is applied with a reduced number of GMRes iterations to 0. The convergence history with respect to this setting is plotted in Figure 6(a). After an initial drop of the residual by about 5 orders of magnitude, the iteration starts to oscillate. Even a reduction of the CFL number from 1000 to 25 does not help. Finally, setting the number of GMRes steps to 200 and thus including an almost exact representation of the residual derivative convergence is enforced. Alternatively, the latter approach can be used directly "from scratch" without major problems, yielding a steady-state solution converged up to machine-accuracy. On the finer mesh having 13.3×10^6 nDoF some work load is shifted into the application of the preconditioner (9) in order to reduce the memory consumption for the GMRes algorithm. The number of Gauss-Seidel sweeps to approximately solve the corresponding linear systems is increased from 5 to 25, while the number of GMRes steps could be reduced to 20. The convergence history is shown in Figure 6(b). A stable drag and lift coef-

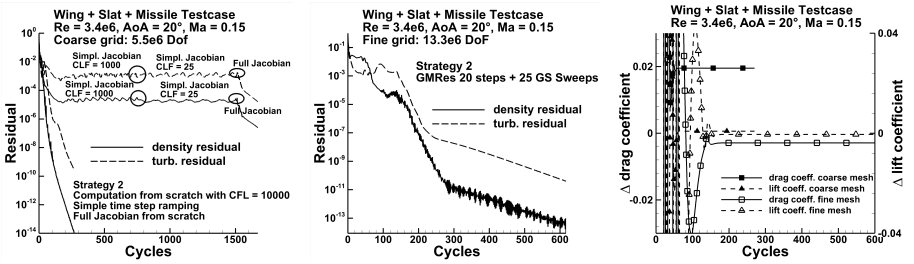

(a) Coarse mesh (b) Fine mesh (c) Delta of drag and lift coefficients

Fig. 6. (a) and (b) Residual convergence for delta-wing with missile; (c) Drag and lift coefficient convergence for delta-wing with missile.

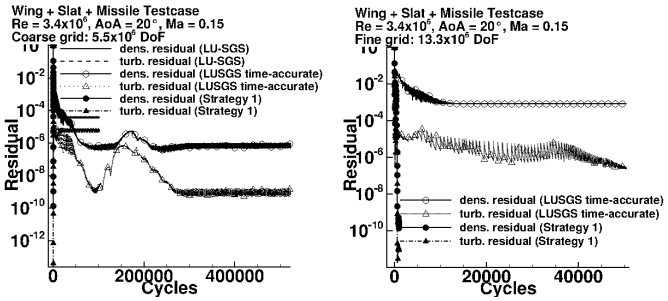

(a) Grid 1, 5.4×10^6 nDoF (b) Grid 2, 13.3×10^6 nDoF

Fig. 7. Residual convergence for delta-wing with missile in highlift configuration using **Strategy 1** from section 2.2.

ficient is given for the coarse mesh after about 70, for the fine mesh after about 150 iterations, corresponding to a residual reduction of about $8 - 9$ orders of magnitude, shown in Figure 6(c). Here, the CFL strategy (10) is used for both, the coarse and the fine mesh. The total computational time to achieve a reduction in the density residual of 14 orders of magnitude on the coarse mesh and 128 domains, i.e. about 43000nDOF per domain, is 8h, and on the fine mesh and 384 domains, i.e. about 34000nDoF per domain, about 24h. Consequently, stable values for lift and drag are obtained after about 6h of computational time on the fine mesh.

For this kind of flows the strongest solution algorithm proposed in this article, that is **Strategy 2** from Section 2.2, is necessary to obtain fully converged solutions. In order to support this statement, a further set of comparisons is made using **Strategy 1** from Section 2.2. Figure 7(a) shows the convergence histories of the LU-SGS method applied directly as multigrid smoother and as a preconditioner for GMRes (**Strategy 1** from Section 2.2) for a steady-state computation and applied as a smoother within an unsteady computation using a BDF2 scheme. For the coarse mesh, the GMRes solver used 200 Krylov vectors with 4 restarts, i. e., the total number of inner linear iterations is 800 or until a residual reduction of 8 orders from the starting linear residual

is achieved. Both the steady-state and time accurate computations stalled, after 4 and 6 orders residual reduction, respectively. However, the approach including the full Jacobian in the GMRes algorithm reached about 10 orders of reduction for the density residual and about 12 for the turbulence residual. For the fine mesh, the convergence of LU-SGS as a single grid relaxation scheme for time-accurate computations is compared with that of the steady-state GMRes-based solver. The number of Krylov vectors and linear iterations are increased to 300 and 1200, respectively. As seen in Figure 7(b), the time-accurate solver again stalled after 3 orders of residual reduction while the proposed steady-state solver according to **Strategy 1** converges with 10 orders of reduction in the density residual. The computational time is 194h on the coarse mesh with 32 partitions and about 231h on the fine mesh with 64 partitions.

4 Conclusion

This article shows results of recent developments targeted at increasing the robustness and applicability of implicit Runge-Kutta smoothers applied to find approximate solutions of the RANS equations. Two ingredients have been identified as crucial. On the one hand, to overcome problems in the start-up phase, while still allowing strongly implicit schemes with large (pseudo-)time steps for final convergence, several stabilization techniques controlling the time step are proposed. On the other hand, a strong smoother (i.e. having a large amount of implicitness) is required to enforce convergence towards a steady state solution, in particular for configurations at the border of the flight envelope. In particular, for the second example shown in Section 3.2, only the method having the largest amount of implicitness had the potential to find a fully converged steady state solution. Incorporating exact derivative information in the linear system to be solved, is an essential first step. Additionally, a suitable preconditioner is required for the GMRes method. For the last example shown in this article, only the preconditioning technique based on a complete Jacobian corresponding to a first order discretization is fully successful, together with a tailored line-implicit iterative linear solver. It should be noted, however, that compared to more simplified methods, these techniques come at the price of increased memory consumption and high computational effort per iteration.
Acknowledgements: Parts of this work have been co-funded by Airbus Defence and Space, Germany. The authors would like to thank Dr. Kolja Elssel for the fruitful discussions, and for providing the second test case, as well as the meshes for both cases.

References

1. Ulrich Trottenberg, C. W. Oosterlee, and Anton Schuller. *Multigrid*. Academic Press, Inc., Orlando, FL, USA, 2001.
2. A. Jameson, W. Schmidt, and E. Turkel. Numerical Solutions of the Euler Equations by Finite Volume Methods Using Runge-Kutta Time-Stepping Schemes. *AIAA Paper, AIAA-81-1259*, 1981.
3. Dimitri J. Mavriplis. Multigrid Strategies for Viscous Flow Solvers on Anisotropic Unstructured Meshes. *ICASE Report No.98-6*, 1998.
4. Pierre Moinier, Jens-Dominik Müller, and Michael B. Giles. Edge-based Multigrid and Preconditioning for Hybrid Grids. *AIAA 99-3339*, 1999.

5. Stefan Langer. Investigation and application of point implicit Runge-Kutta methods to inviscid flow problems. *International Journal for Numerical Methods in Fluids*, 69(2):332–352, 2012.
6. Stefan Langer. Application of a line implicit method to fully coupled system of equations for turbulent flow problems. *Int. J. Comput. Fluid Dyn.*, 27(3):131–150, March 2013.
7. R. C. Swanson, E. Turkel, and C.-C. Rossow. Convergence acceleration of Runge-Kutta schemes for solving the Navier-Stokes equations. *J. Comput. Phys.*, 224(1):365–388, May 2007.
8. Stefan Langer. Preconditioned Newton methods to approximate solutions of the Reynolds averaged Navier-Stokes equations. Technical report, Institut für Aerodynamik und Strömungstechnik, June 2018.
9. P. R. Spalart and S. R. Allmaras. A One-Equation Turbulence Model for Aerodynamic Flows. In *AIAA Computational Fluid Dynamics Conference*, number 1992-439 in Conference Proceeding Series. AIAA, 1992.
10. Steven R. Allmaras, Forrester T. Johnson, and Philippe R. Spalart. Modifications and Clarifications for the Implementation of the Spalart-Allmaras Turbulence Model. In *International Conference on Computational Fluid Dynamics 7, Hawaii*, number ICCFD7-1902 in Conference Proceeding Series, 2012.
11. Stefan Langer. Agglomeration multigrid methods with implicit Runge-Kutta smoothers applied to aerodynamic simulations on unstructured grids. *Journal of Computational Physics*, 277(0):72 – 100, 2014.
12. J. Blazek. *Computational Fluid Dynamics: Principles and Applications*. Elsevier Science Ltd., 2001.
13. Stefan Langer, Axel Schwöppe, and Norbert Kroll. The DLR Flow Solver TAU - Status and Recent Algorithmic Developments. In *Proc. 52nd Aerospace Sciences Meeting, January 2014*, number 2014-0080 in Conference Proceeding Series. AIAA, 2014.
14. Y. Saad. *Iterative Methods for Sparse Linear Systems*. International Thomson Publishing, Boston, 1996.
15. Seokkwan Yoon and Antony Jameson. Lower-upper Symmetric-Gauss-Seidel method for the Euler and Navier-Stokes equations. In *25th AIAA Aerospace Sciences Meeting*, AIAA Paper 1987-0600, Reno, NV, 1987.
16. W. Mulder and Bram van Leer. Experiments with implicit upwind methods for the euler equations. *Journal of Computational Physics*, 59:232–246, 06 1985.
17. D. Hummel. The second international vortex flow experiment (vfe-2). In Rolf Radespiel, Cord-Christian Rossow, and Benjamin Winfried Brinkmann, editors, *Hermann Schlichting – 100 Years*, pages 105–129, Berlin, Heidelberg, 2009. Springer Berlin Heidelberg.
18. D. Hummel and G. Redeker. A new vortex flow experiment for computer code validation. 2001.
19. I. Yamazaki, M. Hoemmen, P. Luszczek, and J. Dongarra. Improving performance of gmres by reducing communication and pipelining global collectives. In *2017 IEEE International Parallel and Distributed Processing Symposium Workshops (IPDPSW)*, pages 1118–1127, 2017.
20. Julio Chu and James M. Luckring. Experimental surface pressure data obtained on 65 deg delta wing across reynolds number and mach number ranges. vol. 3: Medium-radius leading edge. NASA Technical Memorandum 4645, 1996.
21. Stefan Langer. Investigations of a compressible second order finite volume code towards the incompressible limit. *Computers & Fluids*, 149:119 – 137, 2017.